Research Article

Triple-Band MIMO Antenna with Integrated Decoupling Technology

Ruihua Ma ⓘ **, He Huang** ⓘ **, Xiaoping Li** ⓘ **, and Xuelei Wang** ⓘ

Ministry of Education, School of Aerospace Science and Technology, Xidian University, Xi'an 710071, China

Correspondence should be addressed to He Huang; huanghe@xidian.edu.cn

This paper proposes an integrated decoupling method that improves the flexibility of multiport, multiband antenna design and simplifies the antenna structure. First, a dual-band L-type MIMO antenna with center frequencies of 2.6 GHz and 5.6 GHz is created using the neutralization-line decoupling method and then a dual-band L-type MIMO antenna covering the WiFi spectrum (2.3–2.5 GHz and 4.6–5.6 GHz) is created using the type-T branch decoupling technique. After demonstrating the efficacy of neutralization-line and T-branch decoupling technology for L-type antennas, a four-port L-type MIMO antenna covering 4.4–4.9 GHz, 5.4–6.1 GHz, and 7.0–7.4 GHz is proposed by combining the methods of neutralization-line decoupling, T-branch decoupling, and defected ground structure decoupling. This antenna's isolation is higher than 20 dB with ECC less than 0.04.

1. Introduction

In 5G communications, MIMO technology is frequently used. MIMO technology uses multiple antennas for simultaneous transmission and reception [1]. To miniaturize MIMO antennas, the distance between antenna units must be reduced. Each antenna unit is impacted by the currents from others. These complex currents reduce antenna radiation performance. To improve the isolation of the MIMO antennas, decoupling structures must be used.

The decoupling techniques of MIMO antennas should occupy minimal space. These techniques usually etch grooves or add branches to change the current distribution. A mutiband, two-port MIMO antenna is proposed in [2] which loaded a cross-shaped slit and a neutralization line to decoupling. This antenna covers the following four frequency bands: 0.67–7.29 GHz, 8.07–12.11 GHz, 14.07–15.41 GHz, and 16.04–22 GHz. A multiband MIMO antenna that covers the entire terahertz band by its multiple inverted L arms is designed in [3]. The antenna's isolation is higher than 18 dB after loading a meander decoupling structure. A triple-band MIMO antenna using a metamaterial decoupling method is proposed in [4]. $|S_{11}|$ of the presented MIMO antenna is less than -10 dB in 1.1–1.8 GHz, 2.1–3.9 GHz, and 4.1–6 GHz with the isolation better than 10 dB. A vias-based multipath circuit is introduced by [5] for improving the isolation of a dual-band MIMO antenna. With isolation higher than 20 dB, the operation bands cover the WiFi and WLAN bands. A novel decoupling structure was proposed in [6] which included two symmetrical T-type metals on a substrate. The radiated wave, surface wave, and surface current will be prevented by this arrangement.

Due to the limited diversity of dual-port MIMO antennas [7, 8], it is necessary to propose a quad-port MIMO antenna. However, decoupling the four-port MIMO antenna system is challenging because of the increased mutual coupling compared to the dual-port system. In [9], a four-port reconfigurable MIMO antenna is proposed for indoor communication which reduces the interferences and fading effects caused by multipath propagation. This antenna provides RHCP (right-handed circular polarization), LHCP (left-handed circular polarization), and LP (linear polarization) operating in the operation band from 3.1 to 5.1 GHz. The isolation of this antenna is greater than 15 dB and ECC is less than 0.13. In [10], a compact four-port MIMO antenna is presented for vehicular base stations. A cross-π-shaped structure acts as both the reflector and decoupling, which

increases the bandwidth and the isolation. This antenna covers multiple wireless communication bands, including WLAN, 5G, Bluetooth, WiMAX, LTE, and ISM bands with isolation higher than 16 dB. The authors in [11] proposed a four-port annular-ring patch antenna operating in 3.3–5.0 GHz with ECC less than 0.05. Four gap-coupled shorting strips are loaded between the antenna units to achieve better isolation.

In addition, high-performance four-port MIMO antennas operate in multiple frequency bands, which also increases the complexity of decoupling. In the previous papers, only one decoupling method was used, resulting in a complex decoupling structure for the quad-port, multiple-band MIMO antenna. In [12], a four-port MIMO antenna is presented, which utilizes an interlaced lozenge structure for decoupling. This antenna operates in 2.3–2.6 GHz, 3.3–4.4 GHz, and 4.9–5.9 GHz with the isolation higher than 20 dB. A four-port dual-band dielectric resonator-based connected ground MIMO antenna is proposed in [13]. This antenna is used for WLAN and 5G sub-6 GHz communication applications. The isolation degree of this antenna is higher than 20 dB in the operation bands. The authors in [14] presented a dual-band eight-port MIMO antenna operating in the 3.1–3.8 GHz and 4.8–6.0 GHz. The antenna units are connected by a 7.8 mm neutral line to reduce mutual coupling, achieving isolation higher than 17 dB. The authors in [15] demonstrated a four-element MIMO antenna operating in 2.3–3.6 GHz, 5.4–5.8 GHz, and 6.2–12 GHz. By inserting a T-shaped stub into the ground plane, the antenna achieves isolation higher than 15 dB within the operating bands. In addition, the authors in [16] presented a circularly polarized 4-port MIMO antenna for WiFi and WiMAX band communication. Through reasonable space distribution, the mutual coupling is reduced to −18 dB. In [7], a four-port dual-band MIMO antenna is loaded with parasitic decoupling elements to increase the antenna isolation to 18 dB. A low-profile, four-port MIMO antenna operating in the WLAN, n78, and n79 bands is proposed in [17]. The isolation of this antenna is better than 16 dB with ECC less than 0.07. This MIMO antenna has the advantages of small volume, easy integration, and high isolation for 5G terminal applications. A four-pour multiband MIMO antenna is shown in [18]. This antenna operates in 1.5–1.7 GHz and 2.3–6.1 GHz with isolation better than 11 dB. The "Pi-shaped" slot is etched on each antenna unit to achieve a wide bandwidth and reduced mutual coupling. A dual-polarization four-port compact MIMO antenna is designed in [19] which uses L-shaped stubs for decoupling. The proposed antenna operates in three frequency bands with LP (linear polarization) at 1.54 and 2.5 GHz and CP (circular polarized) at 5.63 GHz. To simplify the decoupling structure and improve antenna isolation, this paper proposes an integrated decoupling technology, which is applied to enhance the isolation of a four-port, triple-band MIMO antenna.

The two-port antennas presented in parts A and B consist of two L-type units utilizing T-branch and neutralization-line decoupling techniques, respectively. These two parts demonstrate the efficacy of these decoupling methods for the L-type antennas. In part C, these decoupling technologies, including T-branch, DGS, and neutralization line, are applied to a triple-band antenna by integrating four such antenna units. The proposed triple-band MIMO antenna's isolation exceeds 20 dB in the operating bands of 4.4–4.9 GHz, 5.4–6.1 GHz, and 7.0–7.4 GHz, with ECC <0.04 and CCL <0.2 bits/sec/Hz. These operating bands almost cover the n79, WLAN, and n104 bands.

The comparison of the proposed antenna with multiport, multifrequency MIMO antennas in the recent literature is presented in Table 1. Comparing [7, 9–19], we can clearly see that [13] has a higher gain, while [12] is smaller in size. The antenna suggested in this paper demonstrates superior ECC and isolation. In conclusion, the suggested triple-band MIMO antenna offers comprehensive performance advantages and holds great potential for future applications.

2. Antenna Configuration and Operation Principle

2.1. Dual-Band Antenna Using Neutralization-Line Decoupling Technology. The dual-band MIMO antenna's structure is shown in Figure 1. The dielectric plate material is FR4, and its relative permittivity is 4.4. The dielectric plate length L is 50 mm, the width W is 25 mm, and the thickness h is 0.8 mm. The red part is the top layer of the antenna and the blue part is the bottom layer. The back radiation body of the antenna is used to achieve a low-frequency band, and the high-frequency band is produced by the top microstrip line. The specific values of the antenna structure dimensions are shown in Table 2. The antennas in this work are simulated using Ansoft HFSS.

Figure 2 shows the dual-band MIMO antenna's structure after being added the neutralization lines. The red neutralization line is added between the top microstrip lines to decouple the low-frequency band, and the bending blue neutralization line is added between the back radiators to decouple the high-frequency band. The current distribution on the ground plate is changed by a rectangular slot with a width of 6 mm (L10) and a length of 1 mm (W7). Table 3 displays the antenna's precise values.

The results of the antenna's $|S_{11}|$ and $|S_{21}|$ are shown in Figure 3. The solid lines represent the results after loading the neutralization lines, while the dashed lines depict the results without the neutralization lines. The MIMO antenna operates between 2.6-2.7 GHz and 5.5–5.8 GHz (for $|S_{11}|$ < −10 dB with more than 20 dB isolation). The isolation of the antenna is increased by 9 dB at 2.6 GHz and by 35 dB at 5.6 GHz after loading the neutralization lines.

2.2. Dual-Band MIMO Antenna with the Type-T Branches Decoupling Technology. The structure of the dual-band MIMO antenna is shown in Figure 4. The material of the antenna dielectric plate is FR4. The length L of the dielectric plate is 50 mm, the width W is 26 mm, and the thickness h of the dielectric plate is 0.8 mm. The antenna radiates a low frequency by the bottom blue radiator and a high frequency

TABLE 1: Performance comparison.

References	Size (mm^2)	No. of ports	Bandwidth (GHz)	Isolation (dB)	ECC	Peak gain (dBi)	Technique used
Proposed	50 × 62 1.23λ/1.53λ	4	4.4–4.9 5.4–6.1 7.0–7.4	>20	<0.04	2.5–3.1	Integrate decoupling
[9]	60 × 65 1.25λ/1.36λ	4	3.1–5.1	>15	<0.13	4.85	Connecting stubs
[10]	150 × 150 3.09λ/3.09λ	4	1.9–6.2	>18	<0.03	3.3–6.1	Cross-π-shaped structure
[11]	150 × 150 2.50λ/2.50λ	4	3.3–5.0	>13	<0.05	5.2–6.8	Gap-coupled shorting strip
[12]	38 × 45 0.76λ/0.90λ	4	2.3–2.6 3.3–4.4 4.9–5.9	>19	<0.04	4.0–5.0	Interlaced Lozenges Structure
[13]	60 × 60 1.02λ/1.02λ	4	4.5–4.6 4.9–5.1	>20	<0.04	7.7–8.2	Dielectric resonator
[14]	70 × 150 1.40λ/3.00λ	8	3.1–3.8 4.8–6.0	>17	<0.06	5.6–6.2	Neutral line
[15]	37 × 71 1.48λ/2.84λ	4	2.3–3.6 5.4–5.8 6.2–12.0	>15	<0.04	0.5–1.0	T-branch
[16]	80 × 80 1.45λ/1.45λ	4	3.3–3.8 5.0–5.4	>18	<0.18	5.2–5.5	Space distribution
[7]	58 × 58 1.16λ/1.16λ	4	2.8–3.5 3.9–5.7	>18	<0.07	3.0–5.0	Parasitic metal strips
[17]	60 × 60 1.22λ/1.22λ	4	2.4–2.5 3.7–3.8 4.5–4.6	>16	<0.07	1.1–1.2	Cross slot
[18]	55 × 96 1.12λ/1.95λ	4	1.5–1.7 2.3–6.1	>11	<0.07	4.0–4.1	Rectangular protruding
[19]	60 × 60 1.18λ/1.18λ	4	1.2–1.6 2.3–2.5 5.2–5.9	>15	<0.30	4.2–5.6	L-shaped stubs
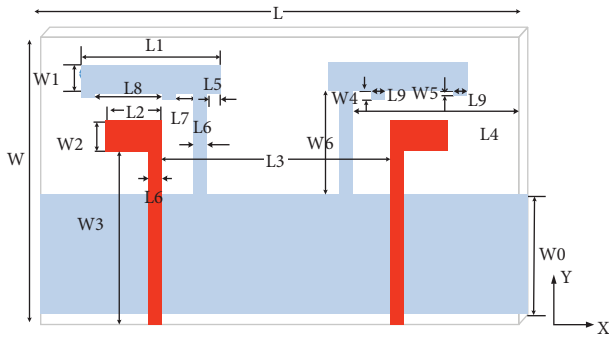
FIGURE 1: Geometry of the dual-band MIMO antenna.

TABLE 2: Parameter values (unit: mm).

Parameters	Numerical value
L	50
W	25
W0	12
L1	13
L2	5
L3	21.6
L4	18
L5	1
L6	1
L8	7
L9	1
L7	2
W1	2
W2	2
W3	16
W4	0.5
W5	0.1
W6	7

by the top red radiator. The specific values of the antenna are shown in Table 4.

Figure 5 shows the dual-band MIMO antenna's structure using type-T branches for decoupling. On the back of the antenna, a short type-T branch given by L4 × W4 is added and a longer branch with a length of L5 is placed above the shorter branch. Two symmetric slits with a length of 2.8 mm and a width of 0.5 mm are etched to change the current distribution of the ground plate [1]. The low-frequency band is decoupled by the longer type-T branch, and the high-frequency band is decoupled by the shorter type-T branch. The specific values of the antenna dimensions are shown in Table 5.
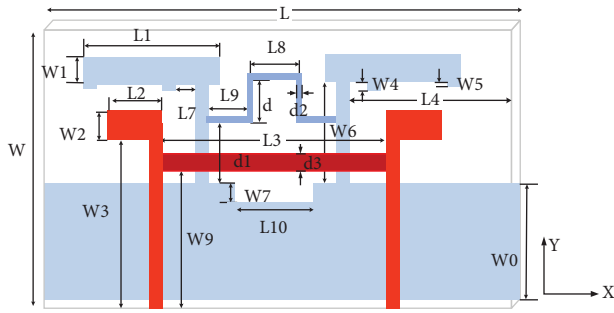
FIGURE 2: Dual-band MIMO antenna model.

TABLE 3: Parameter values (unit: mm).

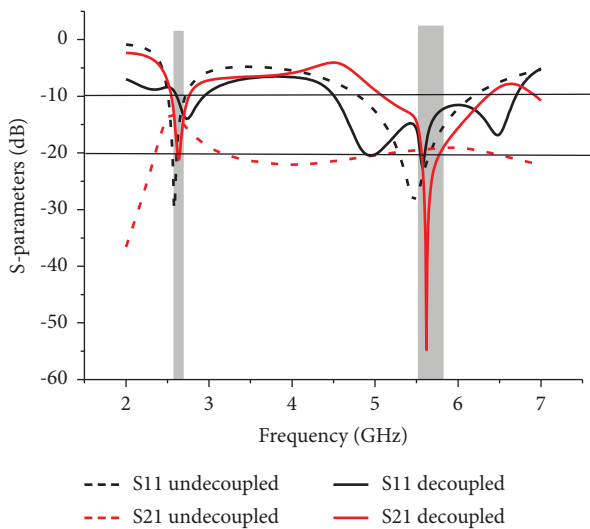| Parameters	Numerical value
L8	4
L9	4
L10	6
W7	1
W8	15
W9	13
d	5
d1	3
d2	0.5
d3	0.8

FIGURE 3: S-parameter simulation results of the dual-band MIMO antenna.

The solid lines represent the results after loading the T-branches, while the dashed lines depict the results without the T-branches. It can be observed from Figure 6 that the operation bands encompass 2.3–2.5 GHz and 4.6–5.6 GHz with more than 20 dB isolation. After adding the type-T branches, the isolation of the antenna at low frequency is increased by 27 dB and at high frequency by 19 dB.
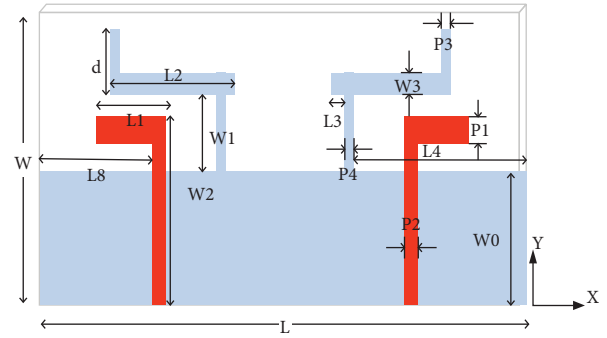
FIGURE 4: Geometry of the dual-band dual-port antenna.

TABLE 4: Parameter values (unit: mm).

Parameters	Numerical value
L	50
W	25
W0	12
L1	6.4
L2	11.8
L3	1
L4	18
d	5.8
W1	7
W2	17.5
W3	2
P1	1.5
P2	1.5
P3	1
P4	1

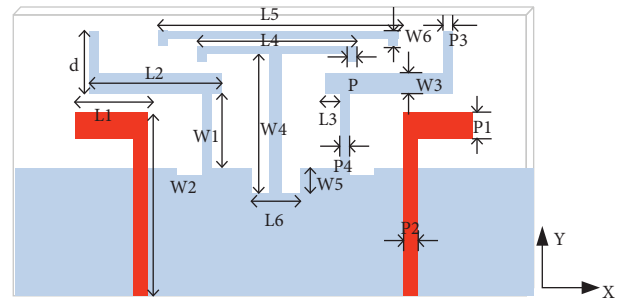

FIGURE 5: Dual-band MIMO antenna model after being added the type-T branches.

TABLE 5: Parameter values (unit: mm).

Parameters	Numerical value
W4	15
W5	3
W6	1
L4	16.5
L5	23
L6	4
P	0.5
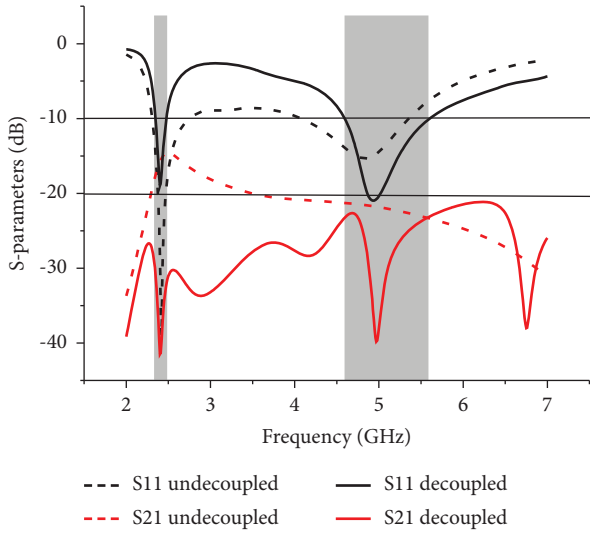
FIGURE 6: Simulation results of the dual-band MIMO antenna with type-T branches added.

FIGURE 7: Integrated decoupled antenna model diagram.

2.3. Integrated Decoupled Triple-Band MIMO Antenna. Figure 7 depicts the structure of the triple-band MIMO antenna utilizing the combined decoupling method. Four antenna units are arranged orthogonally. The antenna has dimensions of 62 mm in length, 50 mm in width, and 0.8 mm in thickness. A ground plate, measuring 50 mm in length and 36 mm in width, connects the four antenna units at the bottom. The T-shaped branches are incorporated into the rectangular slot, and the neutralization line measures 110 mm in length with a width of 0.2 mm. Defective ground structures (DGSs) are placed in the center of the ground plate. Table 6 shows the values of the integrated decoupled antenna structure.

The geometry of DGS is shown in Figure 8. By etching a slot in the rings, the coupling current is trapped after flowing into the defective ground structure. The radius of the ring depends on the operating frequency of the antenna, which is $\lambda/15$. Due to the small coupling current in 7.0–7.4 GHz, the radii of the ring are designed according to the operating frequency of 4.4–4.9 GHz and 5.4–6.1 GHz, so the radii are 3.5 mm and 4.8 mm, respectively. The transmission coefficient of DGS is shown in Figure 9. This DGS effectively blocks the coupling current in 3.8–4.8 GHz and 5.1–6.6 GHz.

The optimization procedure is presented in Table 7. Port 1 serves as the input port. Since the diffraction ability and propagation distance increase with the length of wavelength, the low-frequency electromagnetic wave flow easily to the other port. This is why the isolation between 7.0 and 7.4 GHz is comparatively better. To achieve the desired performance ($|S_{21}| < -20$ dB), it is necessary to reduce the values of $|S_{21}|$, $|S_{31}|$, and $|S_{41}|$ in the 4.4–4.9 GHz and 5.4–6.1 GHz bands, as well as $|S_{31}|$ in the 7.0–7.4 GHz band based on the initial antenna's S-parameters.

Figure 10 displays the current distributions, with port 1 acting as the input port. At frequencies of 4.5 GHz and 5.7 GHz, a portion of the current flows into DGS through the slot and reflects back from the edges of DGS. Another
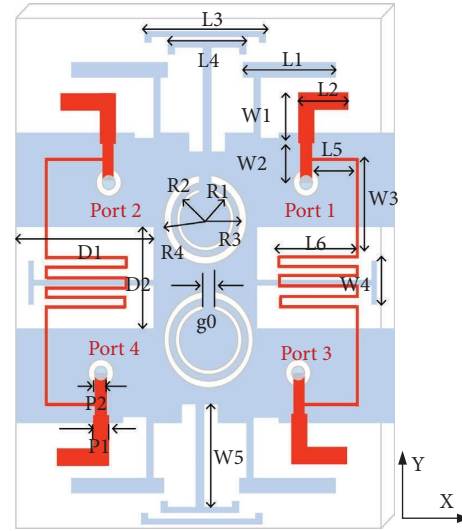
TABLE 6: Parameter values (unit: mm).

Parameters	Numerical value
W1	6.5
W2	6
W3	13
W4	4
W5	15
L1	14
L2	5
L3	17
L4	12
L5	8
L6	10.9
P1	1.5
P2	1
R1	3.5
R2	4
R3	4.8
R4	5.5
g0	2
D1	18
D2	10

portion of the current flows into the T-shaped branches. DGS and type-T branches effectively block the current from entering other ports. In addition, the neutralization lines provide a 180° phase shift that eventually cancels out the coupling current from port 1 to port 3 and port 2 to port 4 in the operation bands.

Figure 11 shows the fabricated prototype of the triple-band antenna. The setup of the anechoic chamber is shown in Figure 12.

In Figure 13, it is evident that the measured results exhibit a great agreement with the simulated results. The antenna operates in the following three frequency bands: 4.4–4.9 GHz, 5.4–6.1 GHz, and 7.0–7.4 GHz, with $|S_{11}| < -10$ dB and $|S_{21}|$, $|S_{31}|$, and $|S_{41}| < -20$ dB. The available bandwidths for these bands are 0.5 GHz, 0.7 GHz, and 0.4 GHz, respectively. As a result, the triple-band antenna's
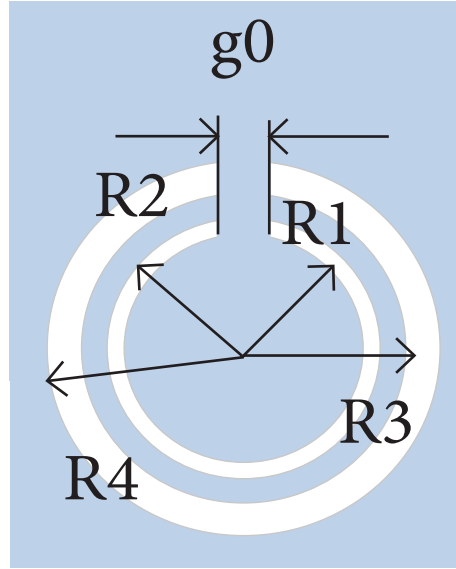
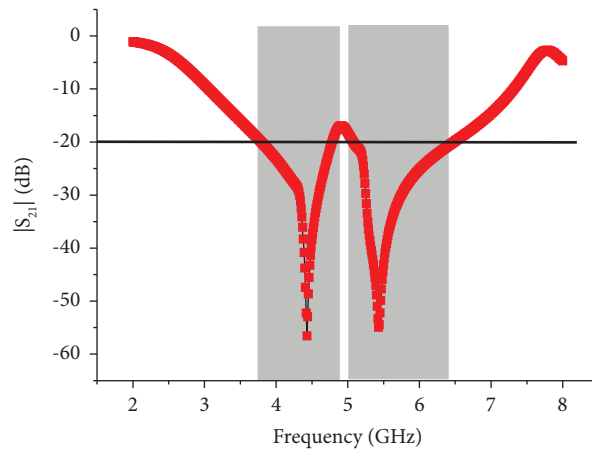FIGURE 8: Geometry of the defected ground structure.

FIGURE 9: Transmission coefficient of the defected ground structure.

isolation is improved by the integrated decoupling technique.

Figure 14 shows the measured and simulated co- and cross-polar components in the E-plane and H-plane when the antenna operates at 4.5, 5.7, and 7.2 GHz, respectively. The antenna is placed horizontally in the x_{oy} plane. At 4.5, 5.7, and 7.2 GHz, the triple-band antenna mainly radiates towards $\varphi = 90°$ and the maximum gain of the proposed antenna is 2.5, 2.8, and 3.1 dBi, respectively, with radiation efficiency above 70%.

The performance parameters of the proposed MIMO antenna are also investigated by calculating the envelope correlation coefficient (ECC) and the channel capacity loss (CCL) [5].

ECC is used to measure the correlation between the antenna elements. ECC is zero when the polarization orientations of the two antennas are parallel to each other [20]. To ensure the efficient operation of each antenna, the specified ECC value of a MIMO system in a wireless communication network is typically less than 0.5 [21]. ECC is calculated using the following equation, where $i, j = 1$–4 [22]:

$$\text{ECC} = \frac{\left| S_{ii}^* S_{ij} + S_{ji}^* S_{jj} \right|^2}{\left(1 - \left| S_{ii} \right|^2 - \left| S_{ji} \right|^2 \right)\left(1 - \left| S_{jj} \right|^2 - \left| S_{ij} \right|^2 \right)}. \quad (1)$$

Figure 15 illustrates the ECC measured outcomes of the proposed MIMO antenna, showing that the ECC values between each pair of ports are less than 0.04 within the operating band.

The maximum range of the transmission rate without loss is indicated by the CCL, which is a crucial parameter for calculating the losses in highly correlated MIMO channels. The recommended CCL limit for a well-designed MIMO system is ≤0.4 bits/s/Hz [23]. The following equations are used to calculate the CCL [24]:
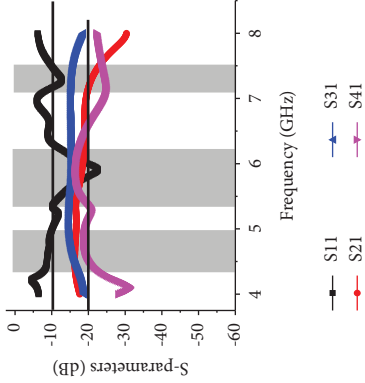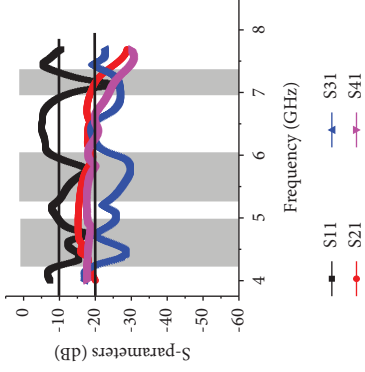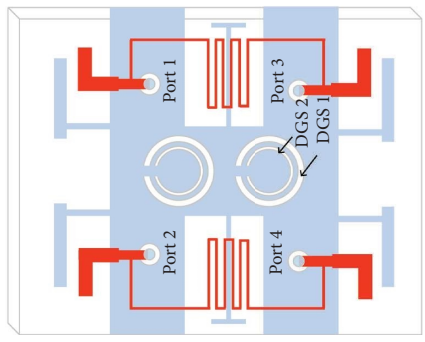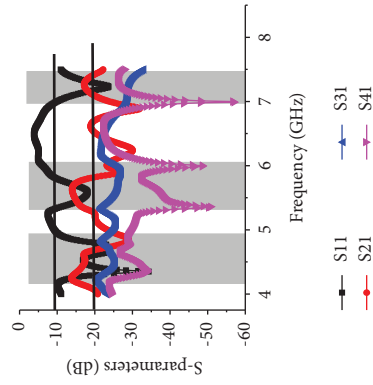
Table 7: Isolation optimization process.

	initial model	$|S_{31}|$ optimization
Optimization process		
S-parameter results		
Principle	The blue branches generate the frequency band of 5.4–6.1 GHz, while the red branches generate the frequency band of 7.0–7.4 GHz. In addition, the neutralization lines enable the antenna to operate within the 4.4–4.9 GHz frequency band	The neutralization lines are designed to introduce a 180° phase shift at 4.5 GHz and 5.7 GHz, effectively cancelling out the coupling current from port 1 to port 3 ($|S_{31}|$). As a result, $|S_{31}|$ is reduced by 13 dB and 15 dB at 4.5 GHz and 5.7 GHz, respectively. Furthermore, the T-branch 3 enhances the isolation between port 1 and port 3 ($|S_{31}|$) by 12 dB in the 7.0–7.4 GHz frequency range

Table 7: Continued.

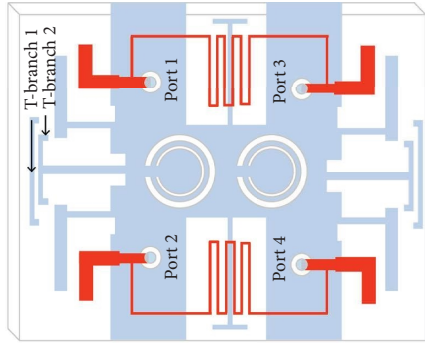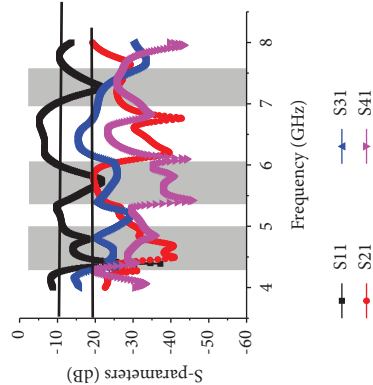|		
Optimization process	$|S_{41}|$ optimization	$|S_{21}|$ optimization
S-parameters		
Principle	The coupling current from port 1 to port 4 ($|S_{41}|$) is effectively blocked by DGS 1 and DGS 2 at the frequencies of 4.4–4.9 GHz and 5.4–6.1 GHz, respectively. $|S_{41}|$ is reduced by 17 dB at 4.3 GHz and reduced by 30 dB at 5.4 GHz	The presence of T-branches significantly decreases $|S_{21}|$ in the operation frequency bands. T-branch 1 improves the isolation between port 1 and port 2 ($|S_{21}|$) by 23 dB in 4.4–4.9 GHz, while T-branch 2 improves the isolation by 5 dB in 5.4–6.1 GHz

(a)

(b)

(c)
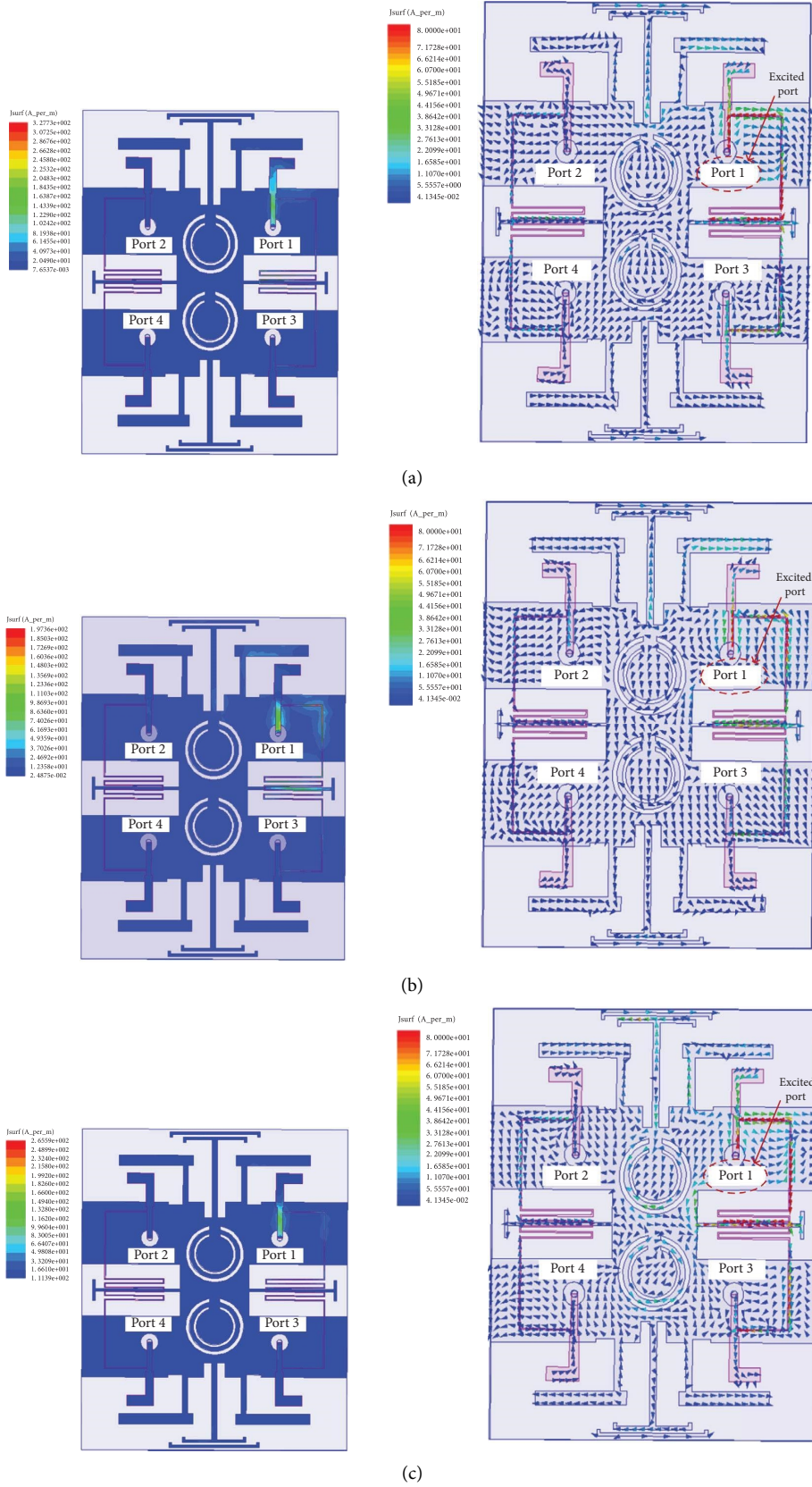
FIGURE 10: Current distribution of the integrated decoupling antenna: (a) 4.5 GHz. (b) 5.7 GHz. (c) 7.2 GHz.

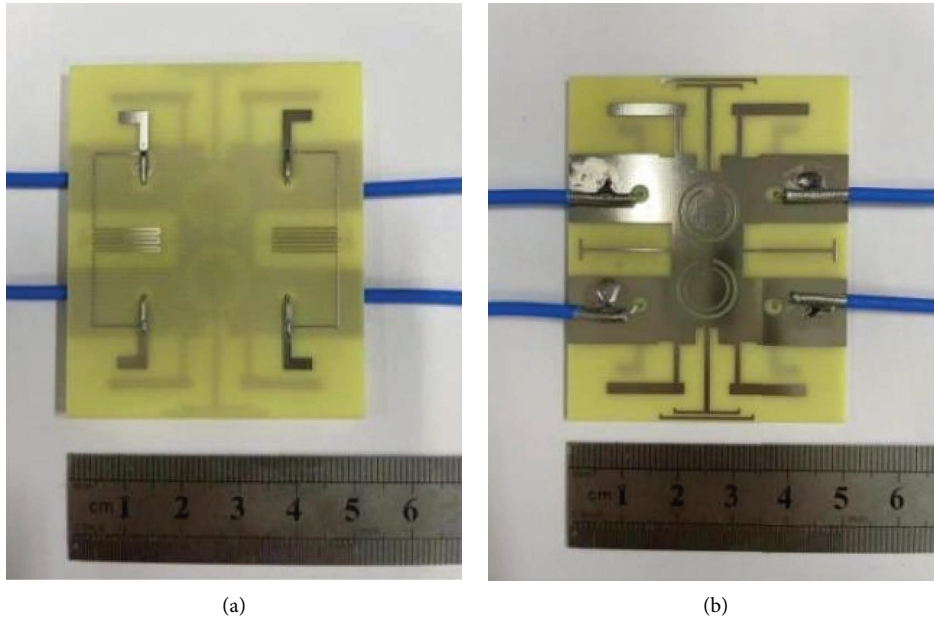(a)   (b)

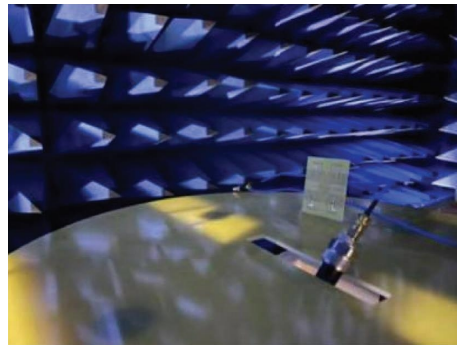FIGURE 11: (a) Antenna's top view. (b) Antenna's bottom view.
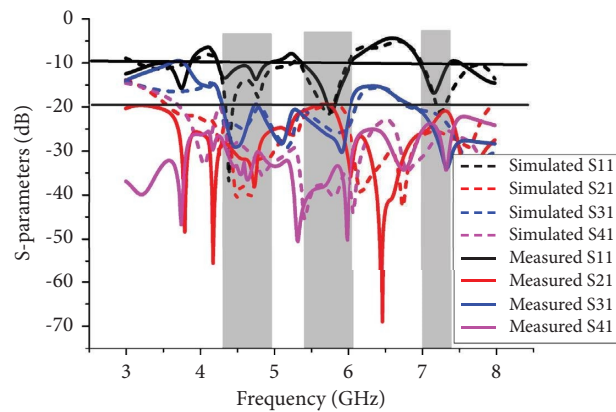

FIGURE 12: Anechoic chamber.

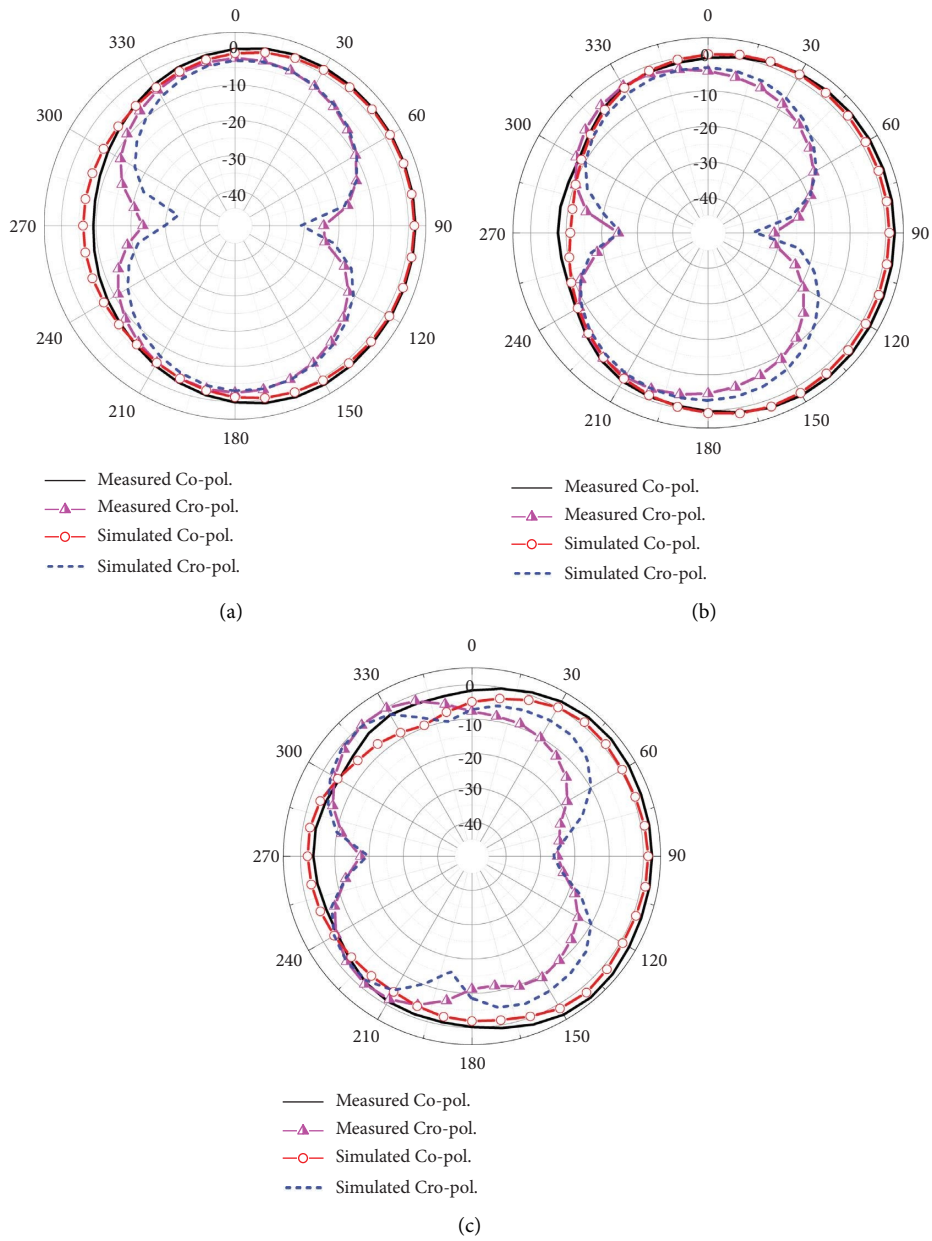FIGURE 13: S-parameter simulated and measured results of the triple-band antenna.

Figure 14: Co- and cross-polar components in the E-plane and H-plane of the integrated decoupled antenna: (a) 4.5 GHz. (b) 5.7 GHz. (c) 7.2 GHz.
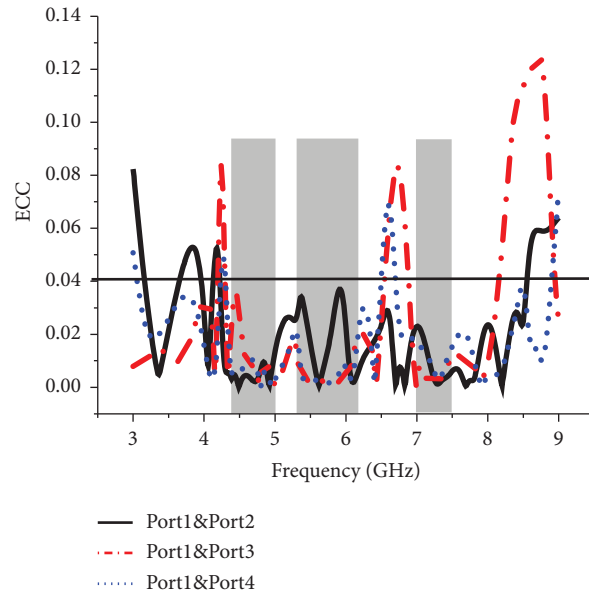
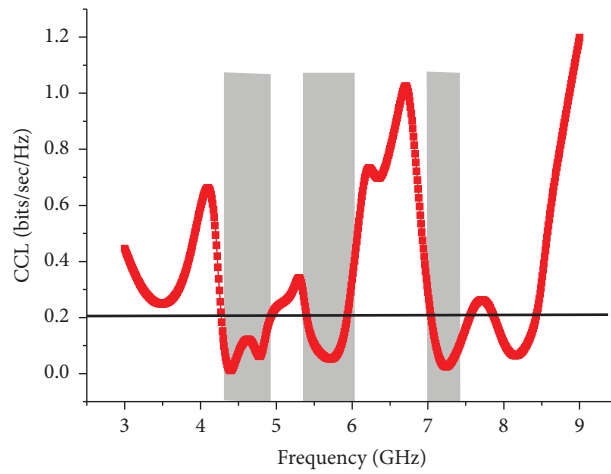FIGURE 15: ECC measured outcomes of the proposed MIMO antenna.

FIGURE 16: CCL measured outcome of the proposed MIMO antenna.

$$\text{CCL} = -\log_2\left|\Psi^R\right|, \tag{2}$$

$$\Psi^R = \begin{bmatrix} \rho_{11} & \rho_{12} & \rho_{13} & \rho_{14} \\ \rho_{21} & \rho_{22} & \rho_{23} & \rho_{24} \\ \rho_{31} & \rho_{32} & \rho_{33} & \rho_{34} \\ \rho_{41} & \rho_{42} & \rho_{43} & \rho_{44} \end{bmatrix}, \tag{3}$$

where Ψ^R is the 4×4 receive signal correlation matrix, $\rho_{ii} = 1 - (\sum_{j=1}^{N}|S_{ij}|^2)$, and $\rho_{ij} = -(S_{ii}^* S_{ij} + S_{ji}^* S_{ij})$ for $i, j = 1, ...,$ 4. In the operation bands depicted in Figure 16, the CCL of the designed antenna is less than 0.2 bits/sec/Hz.

3. Conclusion

This study proposed an integrated decoupling technique for multiband MIMO antennas. First, the paper verifies the efficiency of the T-branches and neutralization lines by two dual-port antennas. Subsequently, a triple-band MIMO antenna is designed to operate at 4.4–4.9 GHz, 5.4–6.1 GHz, and 7.0–7.4 GHz using the integrated decoupling technique. This technique effectively improves antenna isolation and increases antenna design flexibility.

Data Availability

The data used to support the findings of this study are included within the article.

Conflicts of Interest

The authors declare that they have no conflicts of interest.

Acknowledgments

References

[1] X. Wu, "Decoupling technology for dual-band MIMO antenna," pp. 1–65, Shanxi university, Taiyuan, China, 2020, MA thesis.

[2] Z. Wang, W. Mu, M. Yang, and C. Li, "Design of compact multiband MIMO antenna based on ground neutralization line decoupling," *Applied Computational Electromagnetics Society Journal*, vol. 37, no. 6, pp. 702–715, 2022.

[3] B. Ashvanth and B. Partibane, "Multiband characterized high gain MIMO antenna for terahertz applications," *Optical and Quantum Electronics*, vol. 53, no. 8, pp. 460–513, 2021.

[4] S. Roy and U. Chakraborty, "Mutual coupling reduction in a multi-band MIMO antenna using meta-inspired decoupling network," *Wireless Personal Communications*, vol. 114, no. 4, pp. 3231–3246, 2020.

[5] H. V. Singh, D. V. S. Prasad, and S. Tripathi, "Dual-band MIMO antenna decoupling using vias based multipath decoupling circuit," *Microwave and Optical Technology Letters*, vol. 64, no. 4, pp. 770–777, 2022.

[6] Y. Wang, S. Zhang, B. Wang, and A. A. Kishk, "T-type vertical wall for decoupling and pattern correction of patch antenna," *Applied Sciences*, vol. 12, no. 21, pp. 12–11, 2022.

[7] P. Kumar, S. Urooj, and F. Alrowais, "Design and implementation of quad-port MIMO antenna with dual-band elimination characteristics for ultra-wideband applications," *Applied Sciences*, vol. 10, no. 5, pp. 1715–1812, 2020.

[8] A. Ramachandran, S. Valiyaveettil Pushpakaran, M. Pezholil, and V. Kesavath, "A four-port MIMO antenna using concentric square-ring patches loaded with CSRR for high isolation," *Institute of Electrical and Electronics Engineers Antennas and Wireless Propagation Letters*, vol. 15, pp. 1196–1199, 2016.

[9] D. Thangarasu, S. K. Palaniswamy, and R. R. Thipparaju, "Quad port multipolarized reconfigurable MIMO antenna for sub 6 GHz applications," *International Journal of Antennas and Propagation*, vol. 2023, Article ID 8882866, 17 pages, 2023.

[10] W. Wang, Z. Zhao, Q. Sun et al., "Compact quad-element vertically-polarized high-isolation wideband MIMO antenna for vehicular base station," *Institute of Electrical and Electronics Engineers Transactions on Vehicular Technology*, vol. 69, no. 9, pp. 10000–10008, 2020.

[11] K. L. Wong, J. Z. Chen, and W. Y. Li, "Four-port wideband annular-ring patch antenna generating four decoupled waves for 5G multi-input–multi-output access points," *Institute of Electrical and Electronics Engineers Transactions on Antennas and Propagation*, vol. 69, no. 5, pp. 2946–2951, 2021.

[12] J. Kulkarni, A. G. Alharbi, C. Y. D. Sim et al., "Dual polarized, multiband four-port decagon shaped flexible MIMO antenna for next generation wireless applications," *Institute of Electrical and Electronics Engineers Access*, vol. 10, pp. 128132–128150, 2022.

[13] T. Upadhyaya, I. Park, R. Pandey et al., "Aperture-fed quad-port dual-band dielectric resonator-MIMO antenna for sub-6 GHz 5G and WLAN application," *International Journal of Antennas and Propagation*, vol. 2022, Article ID 4136347, 13 pages, 2022.

[14] D. Serghiou, M. Khalily, V. Singh, A. Araghi, and R. Tafazolli, "Sub-6 GHz dual-band 8×8 MIMO antenna for 5G smartphones," *Institute of Electrical and Electronics Engineers Antennas and Wireless Propagation Letters*, vol. 19, no. 9, pp. 1546–1550, 2020.

[15] F. Bahmanzadeh and F. Mohajeri, "Simulation and fabrication of a high-isolation very compact MIMO antenna for ultra-wide band applications with dual band-notched characteristics," *Australian Education Union-international Journal of Electronics and Communications*, vol. 128, Article ID 153505, 2021.

[16] A. K. Dwivedi, A. Sharma, A. K. Singh, and V. Singh, "Design of dual band four port circularly polarized MIMO DRA for WLAN/WiMAX applications," *Journal of Electromagnetic Waves and Applications*, vol. 34, no. 15, pp. 1990–2009, 2020.

[17] Z. Wan, Y. He, Y. Bai, and H. Sun, "Miniaturized, low-profile, triple-band microstrip antenna and its four-antenna module for smartphone applications," *Institute of Electrical and Electronics Engineers Transactions on Antennas and Propagation*, pp. 1–6, 2023.

[18] S. Pourush and R. P. Yadav, "Design of 2x2 multi-band MIMO antenna for wireless applications," in *Proceedings of the 2023 IEEE Wireless Antenna and Microwave Symposium (WAMS)*, pp. 1–5, Ahmedabad, India, March 2023.

[19] A. Mohanty and B. R. Behera, "CMA assisted 4-port compact MIMO antenna with dual-polarization characteristics," *Australian Education Union- International Journal of*

Electronics and Communications, vol. 137, pp. 153794–153812, 2021.

[20] A. A. Ibrahim, J. Machac, and R. M. Shubair, "Compact UWB MIMO antenna with pattern diversity and band rejection characteristics," *Microwave and Optical Technology Letters*, vol. 59, no. 6, pp. 1460–1464, 2017.

[21] Y. Li, C. Y. D. Sim, Y. Luo, and G. Yang, "High-isolation 3.5 GHz eight-antenna mimo array using balanced open-slot antenna element for 5G smartphones," *Institute of Electrical and Electronics Engineers Transactions on Antennas and Propagation*, vol. 67, no. 6, pp. 3820–3830, 2019.

[22] N. Ojaroudi Parchin, Y. I. A. Al-Yasir, H. Jahanbakhsh Basherlou, R. A. Abd-Alhameed, and J. M. Noras, "Orthogonally dual-polarised MIMO antenna array with pattern diversity for use in 5G smartphones," *The Institution of Engineering and Technology Microwaves, Antennas & Propagation*, vol. 14, no. 6, pp. 457–467, 2020.

[23] A. Kumar, A. Q. Ansari, B. K. Kanaujia, and J. Kishor, "High isolation compact four-port MIMO antenna loaded with CSRR for multi-band applications," *Frequenz*, vol. 72, no. 9-10, pp. 415–427, 2018.

[24] K. G. Sujanth Narayan, J. A. Baskaradas, and D. Rajesh Kumar, "Design of a CPW-fed compact MIMO antenna for next generation vehicle to everything (V2X) communication," *Wireless Personal Communications*, vol. 120, no. 3, pp. 2179–2200, 2021.